

Retaining Large and Adjustable Elastic Strains of Kilogram-Scale Nb Nanowires

Shijie Hao,[†] Lishan Cui,^{*,†} Hua Wang,[‡] Daqiang Jiang,[†] Yinong Liu,[§] Jiaqiang Yan,^{||,⊥} Yang Ren,^{*,#} Xiaodong Han,[∇] Dennis E. Brown,[○] and Ju Li^{*,†,□}

[†]State Key Laboratory of Heavy Oil Processing, China University of Petroleum, Beijing 102249, China

[‡]State Key Laboratory for Mechanical Behavior of Materials and Frontier Institute of Science and Technology, Xi'an Jiaotong University, Xi'an 710049, China

[§]School of Mechanical and Chemical Engineering, The University of Western Australia, Crawley, Washington 6009, Australia

^{||}Materials Science and Technology Division, Oak Ridge National Laboratory, Oak Ridge, Tennessee 37831, United States

[⊥]Department of Materials Science and Engineering, University of Tennessee, Knoxville, Tennessee 37996, United States

[#]X-ray Science Division, Argonne National Laboratory, Argonne, Illinois 60439, United States

[∇]Institute of Microstructure and Properties of Advanced Materials, Beijing University of Technology, Beijing 100124, China

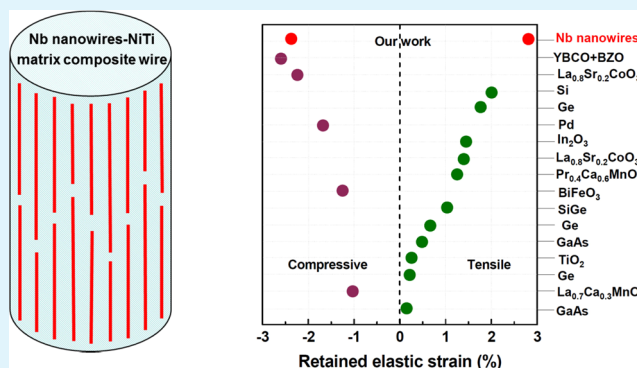
[○]Department of Physics, Northern Illinois University, De Kalb, Illinois 60115, United States

[□]Department of Nuclear Science and Engineering and Department of Materials Science and Engineering, Massachusetts Institute of Technology, Cambridge, Massachusetts 02139, United States

Supporting Information

ABSTRACT: Individual metallic nanowires can sustain ultra-large elastic strains of 4–7%. However, achieving and retaining elastic strains of such magnitude in kilogram-scale nanowires are challenging. Here, we find that under active load, ~5.6% elastic strain can be achieved in Nb nanowires embedded in a metallic matrix deforming by detwinning. Moreover, large tensile (2.8%) and compressive (−2.4%) elastic strains can be retained in kilogram-scale Nb nanowires when the external load was fully removed, and adjustable in magnitude by processing control. It is then demonstrated that the retained tensile elastic strains of Nb nanowires can increase their superconducting transition temperature and critical magnetic field, in comparison with the unstrained original material. This study opens new avenues for retaining large and tunable elastic strains in great quantities of nanowires and elastic-strain-engineering at industrial scale.

KEYWORDS: nanowires, shape memory alloy, high-energy X-ray diffraction, elastic strain, elastic strain engineering



Crystals at ultrahigh levels of elastic strain may exhibit exceptional physical and chemical properties.^{1–8} A commercially successful example is the “strained silicon technology”,^{2,4} where a tensile elastic strain of a few percent is able to enhance the charge carrier mobility several times, which increases the CPU speed so significantly that it has delayed the breakdown of the Moore’s law. However, when attempting to apply elastic strain engineering to energy technologies, one finds that in contrast to information technologies applications where the total mass of active material is tiny (the total weight of strained silicon in a CPU is $\sim 1 \times 10^{-8}$ kg), the total mass of active material to be strain-engineered for energy storage or power transmission has to be much larger. Consider superconducting cables as an example: if we cannot make kilogram- and kilometer-scale strain-engineered superconductor, then elastic strain engineering will not have much real impact.

Much effort has been made to achieve and retain large elastic strains of crystal materials.^{4,7–14} By lattice mismatch between films and substrates, large elastic strains can be retained in films without external load, but it is only applicable to films.^{4,7–10} Near-crack-tip regions in crystal materials can bear large elastic strains, but their volume fractions are too small for meaningful application.^{11,12} Under high hydrostatic pressure, large elastic strains can be produced in gram-scale matters,^{13,14} but it cannot be retained without external load. To date, achieving and retaining large elastic strains of kilogram-scale crystal materials without external load are challenging.

Received: November 10, 2015

Accepted: January 8, 2016

Published: January 8, 2016

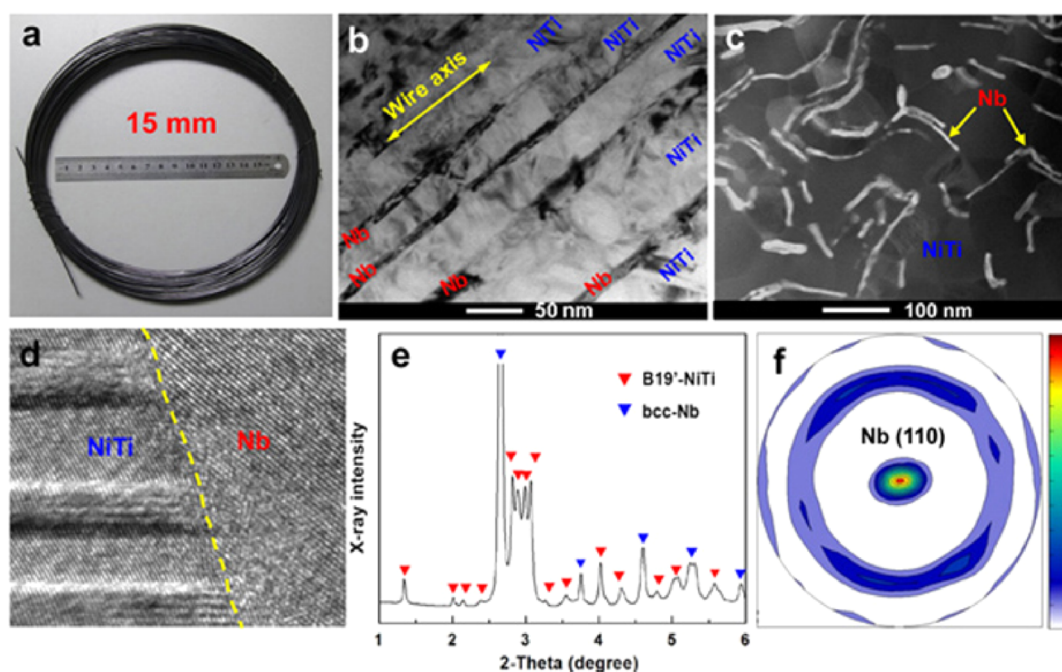


Figure 1. Microstructure of the composite wire. (a) Coil of the composite wire. (b) Bright-field TEM micrograph of a longitudinal-section of the composite wire. (c) Scanning TEM micrograph of a cross-section of the composite wire. (d) High-resolution TEM image of the interface between Nb nanowires and martensitic NiTi matrix with twin substructure. (e) 1D high-energy X-ray diffraction pattern of the composite wire. (f) Nb-[110] pole figure in the wire axial direction.

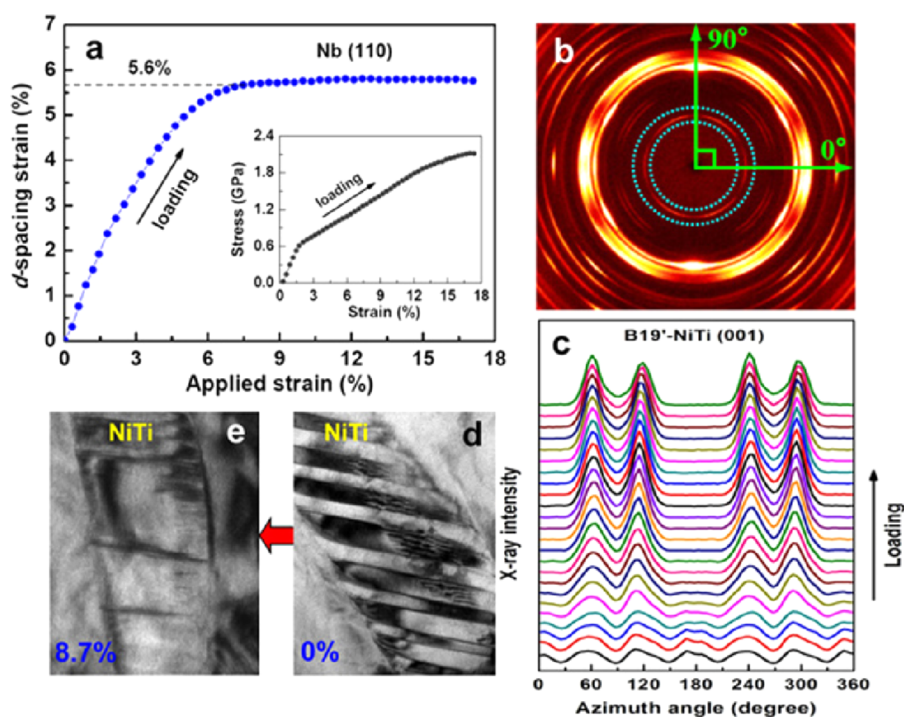


Figure 2. Achieving ultralarge elastic strain of Nb nanowires in martensitic NiTi matrix. (a) Evolution of d -spacing strain with respect to applied strain for the Nb (110) plane perpendicular to the wire axial direction during tensile loading. The inset is the macroscopic stress–strain curve of the composite. (b) 2D high-energy X-ray diffraction pattern of the composite at a certain tensile strain level (1%). (c) Evolution of X-ray diffraction intensity of B19'-NiTi $\langle 001 \rangle$ planes versus the azimuth angle (as determined along the Debye–Scherrer ring indicated in b) during tensile loading. (d, e) TEM micrographs of twin morphologies of the martensitic NiTi matrix before and after a tensile deformation cycle to 8.7%.

Individual metallic nanowires have ultralarge elastic strains, often of the magnitude of 4–7%.^{2,11,15–17} Because of the limitation of using nanowires in their original forms in real applications, it has been conceived to create bulk composites

with these nanowires as fillers. However, the ultralarge elastic strains of nanowires cannot be exploited in conventional composites with the matrices deforming by dislocation slip,^{18–20} as dislocations in the matrix slipping to the matrix/

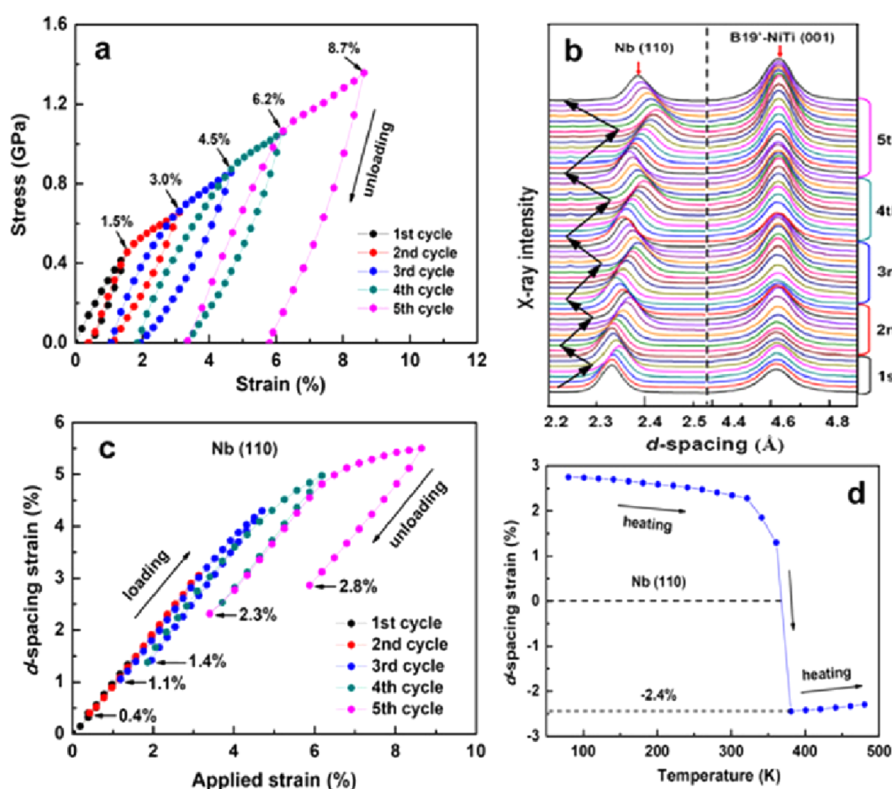


Figure 3. Retaining large elastic strains of great quantity Nb nanowires without external load. (a) Stress–strain curves of multiple-step tensile deformation cycles of the composite. (b) Evolution of high-energy X-ray diffraction peaks for Nb (110) and B19'–NiTi (001) planes through the multiple-step tensile cycles. (c) Evolution of d -spacing strain with respect to applied strain for the Nb (110) plane perpendicular to the wire axial direction during the multiple-step tensile cycles. (d) Evolution of d -spacing strain with respect to temperature for the Nb (110) plane perpendicular to the wire axial direction in the composite predeformed to 8.7% in tension.

nanowire interface cause the atomic-level inelastic shear strain between two adjacent atomic planes exceeding 100% (b/d , where b is Burgers vector and d is interplanar distance, is usually $>100\%$) at the interface,²¹ which easily triggers plasticity in the nanowires. Inspired by this, we hypothesize that the matrix should not deform via sharp microscopic defects such as dislocations or cracks to achieve the ultralarge elastic strain of nanowires in a composite.²² To the best of our knowledge, the shape memory alloy (SMA) in martensite state deforms by detwinning (variant reorientation) that is a collective shearing process of atoms with an atomic-level strain of $\sim 10\%$, and is thus less likely to trigger plasticity in nanowires when the detwinning deformation front of the SMA matrix hits the nanowires. Moreover, the strain reversal of the SMA matrix is smaller than 2% upon tensile unloading which is much smaller than that (4–7%) of the nanowires, which provide an opportunity for the ultralarge elastic strains of nanowires to be achieved first, and later retained in the composite after unloading, in the free-standing condition. This new design paradigm of free-standing composite is illustrated in Figure S1.

To verify the design, we developed an in situ composite wire (Figure 1a) composed of Nb nanowires and martensitic NiTi SMA matrix, which is fabricated by conventional hypo-eutectic ingot casting and wire drawing. Typical microstructure of the composite is shown in Figures 1b–d. The ribbon-shaped Nb nanowires, 4–20 nm in thickness and 20–200 nm in width, are well-dispersed and well-aligned along the axial direction of the composite wire. The Nb nanowires have lengths ranging from 1–100 μm and a mean aspect ratio exceeding 100. The NiTi matrix is in martensitic state at room temperature with twinned

substructure. The volume fraction of the Nb nanowires is about 12%. Chemical analysis of the composite is shown in Figure S2. The high-energy X-ray diffraction pattern of the composite (Figure 1e) can be fully indexed to body-centered cubic Nb and B19'–NiTi phases. Figure 1f shows the pole figure of $\langle 110 \rangle_{\text{Nb}}$ in the wire axial direction. It is evident that the Nb nanowires are strongly oriented with [110] direction parallel to the wire axial direction.

To measure the elastic strains of the embedded Nb nanowires in the martensitic NiTi matrix, in situ synchrotron X-ray diffraction was carried out on the composite during tensile loading (inset of Figure 2a). Figure 2b shows a 2D high-energy X-ray diffraction pattern taken at a certain applied strain (1%). Figure 2c shows the evolution of the X-ray diffraction intensity of B19'–NiTi (001) planes along the Debye–Scherrer ring (as indicated in Figure 2b) recorded at different applied strains. It is seen that the diffraction intensity of B19'–NiTi (001) planes along the Debye–Scherrer ring concentrates approximately equally at 6 locations, separated by $\sim 60^\circ$. Upon loading, the B19'–NiTi (001) diffraction intensity changes significantly to four dominant orientations, indicating that the martensitic NiTi matrix has undergone detwinning (variant reorientation) during deformation.²³ Figures 2d, e show transmission electron microscopy images of the martensitic NiTi matrix before and after a tensile deformation of 8.7% respectively. These further demonstrate that the martensitic NiTi matrix has undergone detwinning during the deformation. Figure 2a shows the evolution of d -spacing strain with respect to applied strain for the Nb (110) planes perpendicular to the loading direction. It is seen that the embedded Nb nanowires reached a maximum

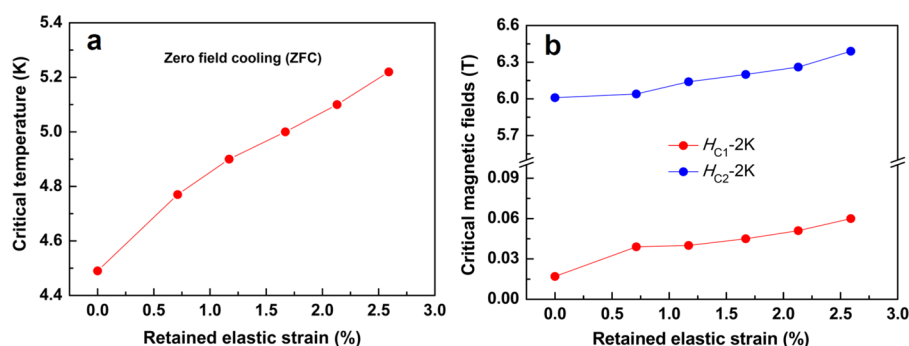


Figure 4. Effect of retained tensile elastic strain on superconducting properties of great quantity Nb nanowires. (a) Dependence of the superconducting transition temperature (T_c , midpoint of the transition curve) of Nb nanowires on the retained tensile elastic strains. (b) Dependence of the critical magnetic fields (the lower critical field H_{c1} and the upper critical field H_{c2}) of Nb nanowires on the retained tensile elastic strains.

tensile elastic strain of 5.6% (at 7.5% applied strain). The elastic strain was induced by the deformation of SMA matrix through detwinning. It is considered that the stress induced at interface is shear stress which resulted in tensile strain in the (110) direction of the nanowire. However, the specific strain transfer mechanism between the martensitic NiTi SMA matrix and the Nb nanowire during tensile loading is still not very clear. This large elastic strain is comparable to those of freestanding nanowires and much larger than those of the nanowires embedded in metal matrices deforming by dislocation slip ($\sim 1.5\%$) (Figure S3).^{19,20}

To determine that the large tensile elastic strain of the Nb nanowires can be retained in the composite after unloading, we performed in situ synchrotron X-ray diffraction on the composite through multiple-step tensile deformation cycles, as shown in Figure 3a. Evolution of X-ray diffraction peaks for Nb (110) and B19'-NiTi (001) planes through the deformation cycles is shown in Figure 3b. Evolution of d -spacing strain with respect to applied strain for the Nb (110) plane perpendicular to the loading direction is shown in Figure 3c. It is observed that tensile elastic strains of 0.4, 1.1, 1.4, 2.3, and 2.8% in the Nb nanowires were retained after deformations to 1.5, 3.0, 4.5, 6.2, and 8.7%, respectively. The dependence of the retained tensile elastic strains in the Nb nanowires on the prior tensile cycle strains of the composite is given in Figure S4. This demonstrates that the magnitude of retained tensile elastic strain in the Nb nanowires can be tailored by adjusting the prior tensile cycle strain of the composite. Moreover, these retained tensile elastic strains (up to 2.8%) in the Nb nanowires are larger than those achieved in thin films on substrates reported in the literature (Figure S5).^{24–29}

The retention of tensile elastic strains in the Nb nanowires after unloading can be understood as following (Figure S1). Upon loading to a tensile strain of ε_y , the martensitic NiTi matrix undergoes a small elastic deformation (O-E) followed by a large detwinning (variant reorientation) deformation (E-F), while the Nb nanowires undergo a large elastic deformation (O-A) followed by a small plastic deformation (A-B). Upon unloading, both the martensitic NiTi matrix and the Nb nanowires recover elastically. However, because the elastic strain of the martensitic NiTi matrix ($\sim 1\%$, Figure S6) is much smaller than that of the Nb nanowires ($\sim 5.6\%$, Figure 2a), the NiTi matrix hinders the full recovery of the Nb nanowires, and the composite equilibrates at point C (Figure S1), causing a large tensile elastic strain in the Nb nanowires (ε_{NW-e}) and a compressive elastic strain in the NiTi matrix (Figure S6) at the end of the unloading.

Large retained compressive elastic strains can also be created in the Nb nanowires by heating the predeformed composite. Figure 3d shows the evolution of the retained elastic strain of the

Nb nanowires in a composite sample predeformed to 8.7% in tension (Figure S7) upon heating. It is seen that the retained tensile elastic strain in the Nb nanowires was released rapidly accompanying the reverse phase transformation (B19' \rightarrow B2) of the NiTi matrix (Figure S8). After heating, a large compressive elastic strain of -2.4% was retained in the Nb nanowires. This retained compressive elastic strain in the Nb nanowires is comparable to those reported for thin films on substrates and embedded nanoinclusions in films,^{24–29} as shown in Figure S5. This can be understood as follows. Upon heating, the martensitic NiTi matrix returned to its initial predeformation shape by the reverse phase transformation (B19' \rightarrow B2) (Figure S8). Because the Nb nanowires underwent a plastic deformation (A-B in Figure S7b) during the predeformation, the plastically deformed Nb nanowires hindered the full shape recovery of the NiTi matrix upon heating, resulting in a large compressive elastic strain in the Nb nanowires and a tensile elastic strain in the NiTi matrix.

Niobium (Nb) is a low-temperature superconductor.³⁰ We herein measured the effect of the retained elastic strains on the superconducting properties of Nb nanowires. Figures S9 and S10 show the superconducting transition curves and the magnetization versus magnetic field (M-H) curves of the Nb nanowires subjected to different retained tensile elastic strains, from $\varepsilon_{[110]} = 0$ to $\varepsilon_{[110]} = 2.6\%$. Dependences of the superconducting transition temperature (T_c) and the critical magnetic fields (H_{c1} and H_{c2}) on the retained tensile elastic strains are shown in Figures 4a and 4b, respectively. It is seen that the T_c , H_{c1} , and H_{c2} of the Nb nanowires significantly increased with increasing the retained tensile elastic strains, demonstrating that the retained tensile elastic strains improve the superconducting properties of great quantities Nb nanowires.

In summary, the ultralarge elastic straining capability of Nb nanowires were exploited in a metal matrix deforming by detwinning. Both the large tensile and compressive elastic strains of Nb nanowires were retained in the free-standing composite after thermal-mechanical treatments, and the retained elastic strains can also be adjusted in magnitude. It is demonstrated that the retained tensile elastic strains can increase the T_c , H_{c1} , and H_{c2} of great quantities of Nb nanowires. This paradigm of locking in large elastic strains in large quantity nanowires in a free-standing composite opens new avenues for retaining large and tunable elastic strains of kilogram-scale crystal materials and exploiting “elastic strain engineering” at industrial scale.

■ ASSOCIATED CONTENT

■ Supporting Information

The Supporting Information is available free of charge on the ACS Publications website at DOI: 10.1021/acsami.5b10840.

Additional information and figure as noted in the text (PDF)

■ AUTHOR INFORMATION

Corresponding Authors

* E-mail: lishancui63@126.com.

*E-mail: ren@aps.anl.gov.

*E-mail: liju@mit.edu.

Notes

The authors declare no competing financial interest.

■ ACKNOWLEDGMENTS

We thank X. Shi and Z. Liu for help in the TEM observations. This work was supported by the Key Program of the NSFC (51231008), the National 973 program of China (2012CB619400), the ARC grant (DP140103805), the NSFC (51471187 and 11474362), Beijing Natural Science Foundation (2152026), and the Science Foundation of China University of Petroleum, Beijing (2462013YJRC005). The use of the Advanced Photon Source was supported by the US Department of Energy, Office of Science, and Office of Basic Energy Science under Contract No. DE-AC02-06CH11357. J. Yan acknowledges support from the US Department of Energy, Office of Science, Basic Energy Sciences, Materials Sciences and Engineering Division.

■ REFERENCES

- (1) Li, J.; Shan, Z. W.; Ma, E. Elastic Strain Engineering for Unprecedented Materials Properties. *MRS Bull.* **2014**, *39*, 108–117.
- (2) Zhu, T.; Li, J. Ultra-Strength Materials. *Prog. Mater. Sci.* **2010**, *55*, 710–757.
- (3) Hicks, C. W.; Brodsky, D. O.; Yelland, E. A.; Gibbs, A. S.; Bruin, J. A. N.; Barber, M. E.; Edkins, S. D.; Nishimura, K.; Yonezawa, S.; Maeno, Y.; Mackenzie, A. P. Strong Increase of T_c of Sr_2RuO_4 Under Both Tensile and Compressive Strain. *Science* **2014**, *344*, 283–285.
- (4) Jacobsen, R. S.; Andersen, K. N.; Borel, P. I.; Fage-Pedersen, J.; Frandsen, L. H.; Hansen, O.; Kristensen, M.; Lavrinenko, A. V.; Moulin, G.; Ou, H.; Peucheret, C.; Zsigri, B.; Bjarklev, A. Strained Silicon as a New Electro-Optic Material. *Nature* **2006**, *441*, 199–202.
- (5) Levy, N.; Burke, S. A.; Meaker, K. L.; Panlasigui, M.; Zettl, A.; Guinea, F.; Neto, A. H. C.; Crommie, M. F. Strain-Induced Pseudo-Magnetic Fields Greater Than 300 T in Graphene Nanobubbles. *Science* **2010**, *329*, 544–547.
- (6) Cao, J.; Ertekin, E.; Srinivasan, V.; Fan, W.; Huang, S.; Zheng, H.; Yim, J. W. L.; Khanal, D. R.; Ogletree, D. F.; Grossman, J. C.; Wu, J. Strain Engineering and One-Dimensional Organization of Metal-Insulator Domains in Single-Crystal Vanadium Dioxide Beams. *Nat. Nanotechnol.* **2009**, *4*, 732–737.
- (7) Strasser, P.; Koh, S.; Anniyev, T.; Greeley, J.; More, K.; Yu, C. F.; Liu, Z. C.; Kaya, S.; Nordlund, D.; Ogasawara, H.; Toney, M. F.; Nilsson, A. Lattice-Strain Control of the Activity in Dealloyed Core-Shell Fuel Cell Catalysts. *Nat. Chem.* **2010**, *2*, 454–460.
- (8) Schlom, D. G.; Chen, L. Q.; Eom, C. B.; Rabe, K. M.; Streiffer, S. K.; Triscone, J. M. Strain Tuning of Ferroelectric Thin Films. *Annu. Rev. Mater. Res.* **2007**, *37*, 589–626.
- (9) MaCmanus-Driscoll, J. L.; Zerrer, P.; Wang, H. Y.; Yang, H.; Yoon, J.; Fouchet, A.; Yu, R.; Blamire, M. G.; Jia, Q. X. Strain Control and Spontaneous Phase Ordering in Vertical Nanocomposite Heteroepitaxial Thin Films. *Nat. Mater.* **2008**, *7*, 314–320.
- (10) Jang, H. W.; Baek, S. H.; Ortiz, D.; Folkman, C. M.; Das, R. R.; Chu, Y. H.; Shafer, P.; Zhang, J. X.; Choudhury, S.; Vaithyanathan, V.; Chen, Y. B.; Felker, D. A.; Biegalski, M. D.; Rzchowski, M. S.; Pan, X. Q.; Schlom, D. G.; Chen, L. Q.; Ramesh, R.; Eom, C. B. Strain-Induced Polarization Rotation in Epitaxial (001) $BiFeO_3$ Thin Films. *Phys. Rev. Lett.* **2008**, *101*, 107602.
- (11) Yue, Y. H.; Liu, P.; Zhang, Z.; Han, X. D.; Ma, E. Approaching the Theoretical Elastic Strain Limit in Copper Nanowires. *Nano Lett.* **2011**, *11*, 3151–3155.
- (12) Rice, J. The Elastic-Plastic Mechanics of Crack Extension. *Int. J. Fract. Mech.* **1968**, *4*, 41–47.
- (13) Duffy, T. S.; Shen, G.; Heinz, D. L.; Shu, J.; Ma, Y.; Mao, H.-K.; Hemley, R. J.; Singh, A. K. Lattice Strains in Gold and Rhenium under Nonhydrostatic Compression to 37 GPa. *Phys. Rev. B: Condens. Matter Mater. Phys.* **1999**, *60*, 15063–15073.
- (14) Singh, A. K.; Balasingh, C.; Mao, H.-k.; Hemley, R. J.; Shu, J. Analysis of Lattice Strains Measured under Nonhydrostatic Pressure. *J. Appl. Phys.* **1998**, *83*, 7567–7575.
- (15) Richter, G.; Hillerich, G.; Gianola, D. S.; Monig, R.; Kraft, O.; Volkert, C. A. Ultrahigh Strength Single Crystalline Nanowhiskers Grown by Physical Vapor Deposition. *Nano Lett.* **2009**, *9*, 3048–3052.
- (16) Wong, E. W.; Sheehan, P. E.; Lieber, C. M. Nanobeam Mechanics: Elasticity, Strength and Toughness of Nanorods and Nanotubes. *Science* **1997**, *277*, 1971–1975.
- (17) Tian, L.; Cheng, Y. Q.; Shan, Z. W.; Li, J.; Wang, C. C.; Han, X. D.; Sun, J.; Ma, E. Approaching the Ideal Elastic Limit of Metallic Glasses. *Nat. Commun.* **2012**, *3*, 609.
- (18) Dzenis, Y. Structural Nanocomposites. *Science* **2008**, *319*, 419–420.
- (19) Vidal, V.; Thilly, L.; Van Petegem, S.; Stuhr, U.; Lecouturier, F.; Renault, P. O.; Van Swynghevoen, H. Plasticity of Nanostructured Cu-Nb-based Wires: Strengthening Mechanisms Revealed by in Situ Deformation under Neutrons. *Scr. Mater.* **2009**, *60*, 171–174.
- (20) Scheuerlein, C.; Stuhr, U.; Thilly, L. In-Situ Neutron Diffraction under Tensile Loading of Powder-in-Tube Cu/Nb₃Sn Composite Wires: Effect of Reaction Heat Treatment on Texture, Internal Stress State, and Load Transfer. *Appl. Phys. Lett.* **2007**, *91*, 042503.
- (21) Ogata, S.; Li, J.; Yip, S. Ideal Pure Shear Strength of Aluminum and Copper. *Science* **2002**, *298*, 807–811.
- (22) Hao, S. J.; Cui, L. S.; Jiang, D. Q.; Han, X. D.; Ren, Y.; Jiang, J.; Liu, Y. N.; Liu, Z. Y.; Mao, S. C.; Wang, Y. D.; Li, Y.; Ren, X. B.; Ding, X. D.; Wang, S.; Yu, C.; Shi, X. B.; Du, M. S.; Yang, F.; Zheng, Y. J.; Zhang, Z.; Li, X. D.; Brown, D. E.; Li, J. A Transforming Metal Nanocomposite with Large Elastic Strain, Low Modulus, and High Strength. *Science* **2013**, *339*, 1191–1194.
- (23) Otsuka, K.; Ren, X. Physical Metallurgy of Ti-Ni-Based Shape Memory Alloys. *Prog. Mater. Sci.* **2005**, *50*, 511–678.
- (24) Cai, Z. H.; Kuru, Y.; Han, J. W.; Chen, Y.; Yildiz, B. Surface Electronic Structure Transitions at High Temperature on Perovskite Oxides: The Case of Strained $La_{0.8}Sr_{0.2}CoO_3$ Thin Films. *J. Am. Chem. Soc.* **2011**, *133*, 17696–17704.
- (25) Hobart, K. D.; Kub, F. J.; Fatemi, M.; Twigg, M. E.; Thompson, P. E.; Kuan, T. S.; Inoki, C. K. Compliant Substrates: A Comparative Study of the Relaxation Mechanisms of Strained Films Bonded to High and Low Viscosity Oxides. *J. Electron. Mater.* **2000**, *29*, 897–900.
- (26) Zeches, R. J.; Rossell, M. D.; Zhang, J. X.; Hatt, A. J.; He, Q.; Yang, C. H.; Kumar, A.; Wang, C. H.; Melville, A.; Adamo, C.; Sheng, G.; Chu, Y. H.; Ihlefeld, J. F.; Erni, R.; Ederer, C.; Gopalan, V.; Chen, L. Q.; Schlom, D. G.; Spaldin, N. A.; Martin, L. W.; Ramesh, R. A Strain-Driven Morphotropic Phase Boundary in $BiFeO_3$. *Science* **2009**, *326*, 977–980.
- (27) Zhang, K. H. L.; Lazarov, V. K.; Veal, T. D.; Oropeza, F. E.; McConville, C. F.; Egdell, R. G.; Walsh, A. Thickness Dependence of the Strain, Band Gap and Transport Properties of Epitaxial In_2O_3 Thin Films Grown on Y-Stabilised ZrO_2 (111). *J. Phys.: Condens. Matter* **2011**, *23*, 334211.
- (28) Infante, I. C.; Sanchez, F.; Fontcuberta, J.; Wojcik, M.; Jedryka, E.; Estrade, S.; Peiro, F.; Arbiol, J.; Laukhin, V.; Espinos, J. P. Elastic and Orbital Effects on Thickness-Dependent Properties of Manganite Thin Films. *Phys. Rev. B: Condens. Matter Mater. Phys.* **2007**, *76*, 224415.

(29) Horide, T.; Kitamura, T.; Ichinose, A.; Matsumoto, K. Elastic Strain Evolution in Nanocomposite Structure of $\text{YBa}_2\text{Cu}_3\text{O}_7+\text{BaZrO}_3$ Superconducting Films. *Jpn. J. Appl. Phys.* **2014**, *53*, 083101.

(30) Laverick, C. TMS Symposium on Niobium and Niobium Alloys in Superconducting Applications Niobium demand and superconductor applications: An overview. *J. Less-Common Met.* **1988**, *139*, 107–122.

Supporting Information for:

Retaining Large and Adjustable Elastic Strains of Kilogram-Scale

Nb Nanowires

Shijie Hao,[†] Lishan Cui,^{*†} Hua Wang,[‡] Daqiang Jiang,[†] Yinong Liu,[§] Jiaqiang Yan,^{||,⊥}

Yang Ren,^{*#} Xiaodong Han,[∇] Dennis. E. Brown,[°] and Ju Li^{*†,||}

[†]State Key Laboratory of Heavy Oil Processing, China University of Petroleum, Beijing 102249, China

[‡]State Key Laboratory for Mechanical Behavior of Materials and Frontier Institute of Science and Technology, Xi'an Jiaotong University, Xi'an 710049, China

[§]School of Mechanical and Chemical Engineering, The University of Western Australia, Crawley, WA 6009, Australia

^{||}Materials Science and Technology Division, Oak Ridge National Laboratory, Oak Ridge, TN 37831, USA

[⊥]Department of Materials Science and Engineering, University of Tennessee, Knoxville, TN 37996, USA

[#]X-ray Science Division, Argonne National Laboratory, Argonne, Illinois 60439, USA

[∇]Institute of Microstructure and Properties of Advanced Materials, Beijing University of Technology, Beijing 100124, China

[°]Department of Physics, Northern Illinois University, De Kalb, Illinois 60115, USA

^{||}Department of Nuclear Science and Engineering and Department of Materials Science and Engineering, Massachusetts Institute of Technology, Cambridge, Massachusetts 02139, USA

Corresponding Authors

*E-mail: lishancui63@126.com, *E-mail: ren@aps.anl.gov, *E-mail: liju@mit.edu

1. Experiment Section

1.1 Material preparation: An alloy ingot of 100 mm in diameter and 25 kg in weight with a composition of Ni₄₅Ti₄₅Nb₁₀ (atomic %) was prepared by vacuum induction melting. The raw materials used were of commercial purity Ni (99.96 wt.%), Ti (99.90 wt.%) and Nb (99.99 wt.%). The ingot was hot-forged at 850 °C into a rod of 8 mm in diameter and further hot-drawn at 750 °C into a thick wire of 2 mm in diameter. Then the hot-drawn wire was cold-drawn into thin wire of 0.5 mm in diameter at room temperature with intermediate annealing at 700 °C. The test samples were cut from the cold-drawn wire and subsequently annealed at 500 °C for 20 min followed by air cooling.

1.2 *In situ* synchrotron X-ray diffraction measurement: *In situ* synchrotron X-ray diffraction measurements were performed at the 11-ID-C beamline of the Advanced Photon Source at Argonne National Laboratory. High-energy X-rays of 114.76 keV energy and 0.6 mm × 0.6 mm beam size were used to obtain two-dimensional (2-D) diffraction patterns in the transmission geometry using a Perkin-Elmer large area detector placed downstream at 1.8 m away from the sample. The 2-D diffraction patterns were collected during tensile deformation using a home-made mechanical testing device. Gaussian fits were used to determine diffraction peak positions. Error of the *d*-spacing strain measurement is estimated to be smaller than 0.1%. Tensile tests were performed using an Instron testing machine at a strain rate of $1 \times 10^{-4} \text{ s}^{-1}$ and the total elongation of the gauge length was measured with a static axial clip-on extensometer. The heating experiment was performed using a Linkam thermal stage at a heating rate of 5°C/min.

1.3 Transmission electron microscope measurement: Microstructure and chemical composition of the composite were analyzed using a FEI Tecnai G2 F20 transmission electron microscope equipped with an energy dispersive X-ray spectroscopic analyzer operated at a voltage of 200 kV.

1.4 Superconducting property measurement: The temperature dependence of magnetic susceptibility was measured in both zero-field-cooling (ZFC) and field-cooling (FC) modes with a field of 10 Oe using a Quantum Design (QD) magnetic properties measurement system (MPMS).

2. Figures

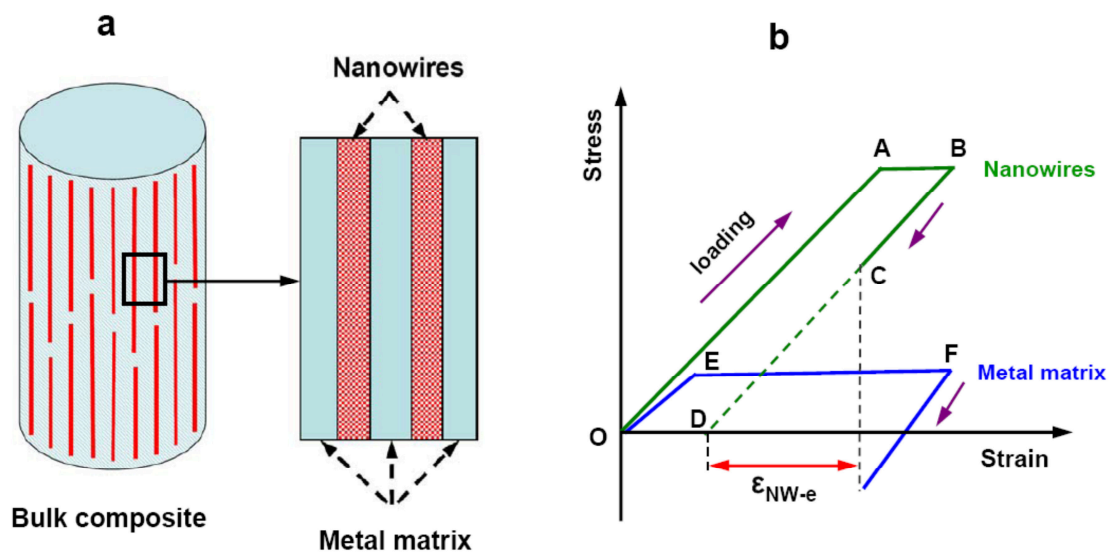


Figure S1. (a) Schematic of the bulk composite composed of the nanowires with large elastic strain limit and the metal matrix deformed by detwinning with small elastic strain

limit. (b) Schematic of the deformation behavior of the nanowires and the metal matrix during the tensile loading and unloading of bulk composite.

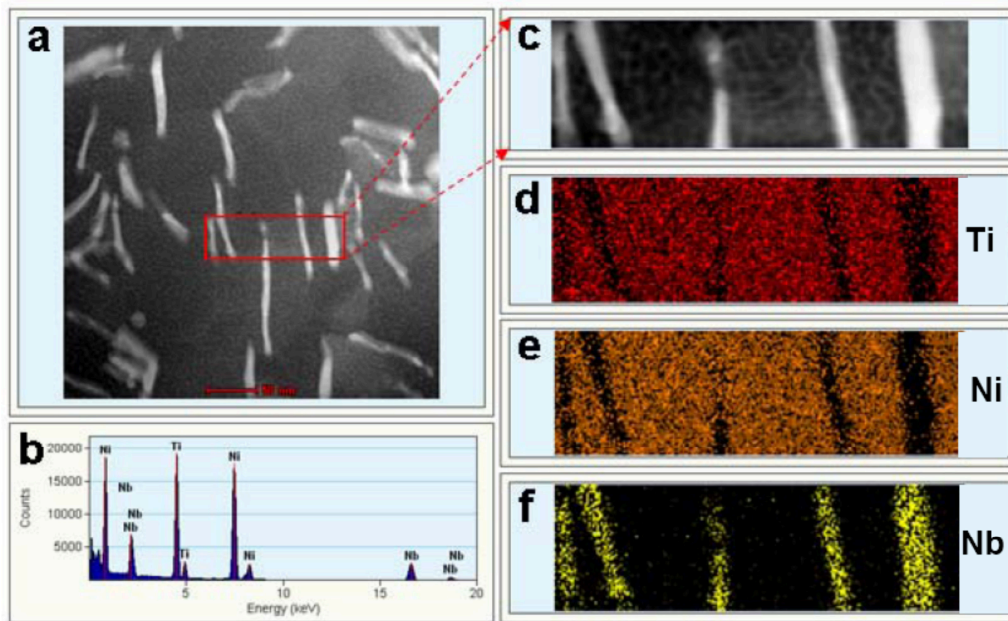


Figure S2. Energy dispersive analysis on the chemical composition distribution of the composite wire. (a) Low-magnification STEM image of the cross section of composite wire (bright regions: cross sections of Nb nanowires; dark regions: NiTi matrix). (b) Energy dispersive X-ray spectrum of the composite. (c) Enlarged view of the region in the red frame in Fig. S2-a. (d) Mapping of titanium. (e) Mapping of nickel. f, Mapping of niobium. The Nb nanowires contain 86.1Nb, 10.7Ti and 3.2Ni (at. %), and the NiTi matrix contains 48.1Ti, 50.5Ni and 1.4Nb (at.%).

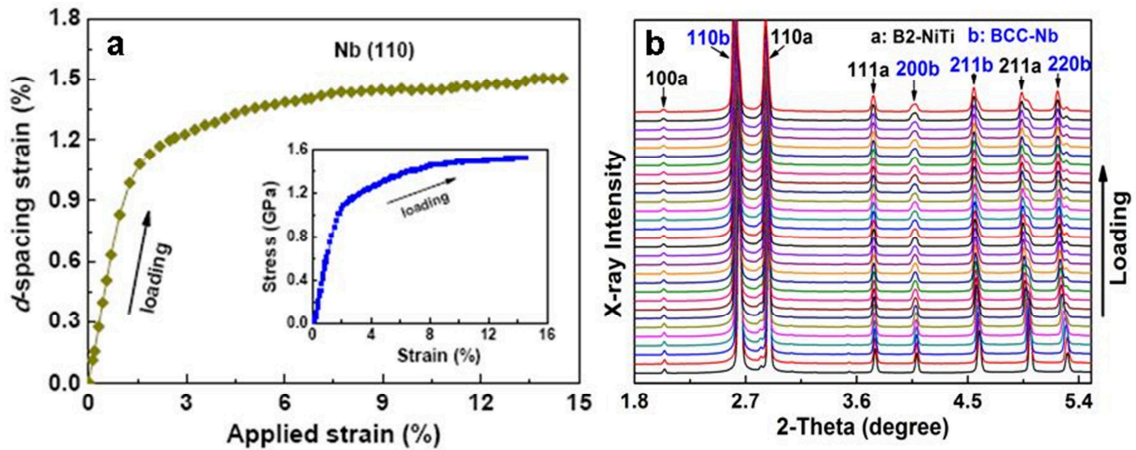


Figure S3. Elastic strain limit of the Nb nanowires embedded in the NiTi matrix plastically deformed by dislocation slip. (a) Evolution of d -spacing strain with respect to applied strain for the Nb (110) plane perpendicular to the loading direction during tensile loading. Inset is the tensile stress-strain curve of the composite obtained at 200 °C. (b) One-dimensional high-energy X-ray diffraction patterns of the composite obtained during tensile loading at 200 °C.

Note: As a direct comparison, *in situ* synchrotron X-ray diffraction was carried out on the composite wire during tensile loading at 200 °C (inset of Fig. S3-a). Fig. S3-b shows that the intensities of all diffraction peaks of the B2-NiTi phase almost remain constant and no other new diffraction peak appears throughout the tensile loading, demonstrating that the B2-NiTi matrix underwent plastic deformation by dislocation slip at 200 °C. The evolution of d -spacing strain with respect to applied strain for the Nb (110) perpendicular to loading direction (Fig. S3-a) shows that the Nb nanowires in the NiTi matrix plastically deformed by dislocation slip merely exhibit the elastic strain limit of 1.5% which is much less than that of the Nb nanowires in the martensitic NiTi matrix deformed by detwinning (~5.6%).

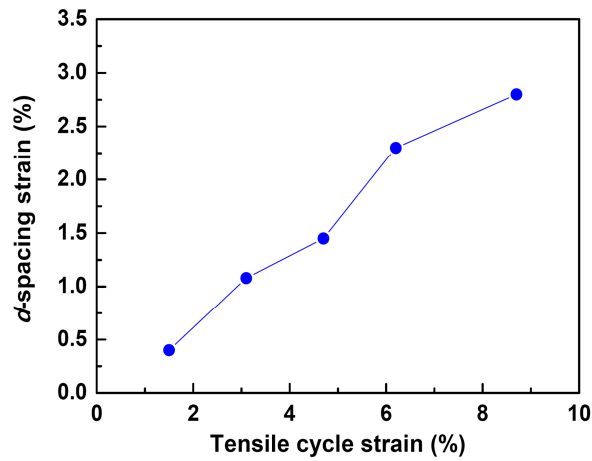


Figure S4. The dependence of the retained tensile elastic strains in the Nb nanowires on the prior tensile cycle strains of the composite.

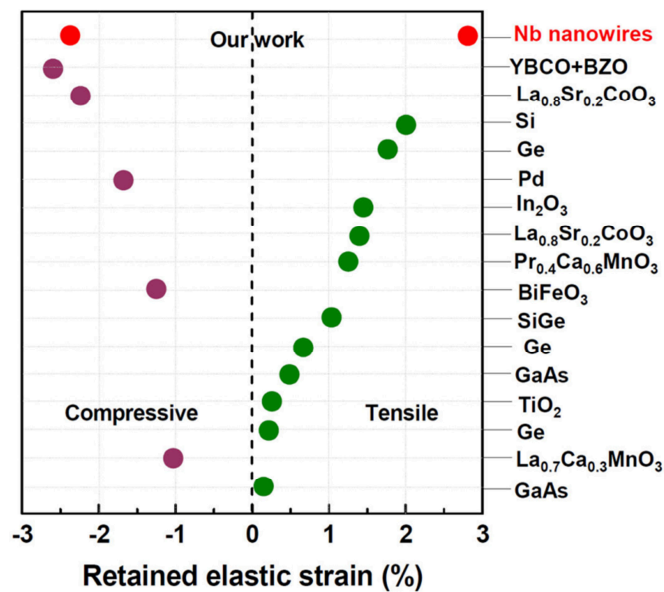


Figure S5. Comparison of the retained tensile and compressive elastic strains of large quantity Nb nanowires in the composite without external load and those of the reported thin films on substrates and embedded nanoinclusions in films.

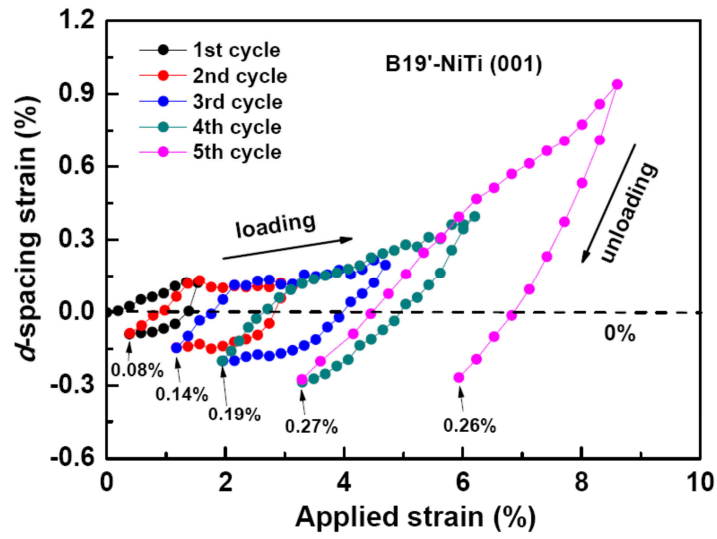


Figure S6. Evolution of d -spacing strain with respect to applied strain for the B19'-NiTi (001) plane perpendicular to the loading direction through the multiple-step tensile cycles of the composite (Figure 3a).

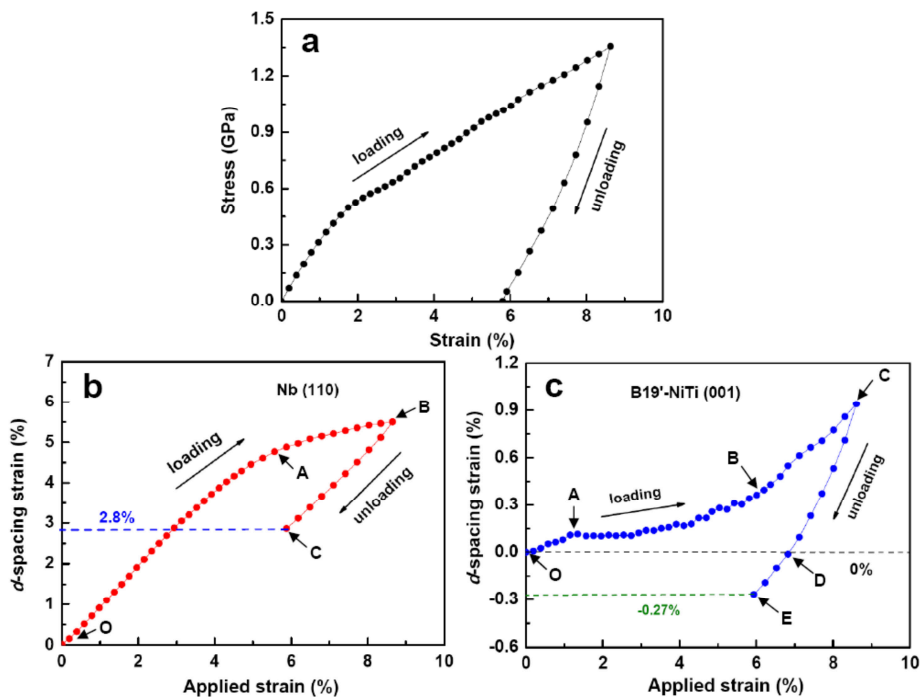


Figure S7. *In situ* synchrotron study of the composite through a tensile cycle of 8.7%. (a)

Tensile cycle stress-strain curve of 8.7%. (b-c) Evolutions of d -spacing strain with respect to applied strain for the Nb (110) and B19'-NiTi (001) planes perpendicular to the loading direction in the tensile cycle of 8.7%.

Note: Upon loading, the Nb nanowires (Figure S7-b) underwent a large tensile elastic deformation (O-A) and a tensile plastic deformation (A-B), the martensitic NiTi matrix (Figure S7-c) underwent a small tensile elastic deformation (O-A), detwinning deformation (A-B), a tensile elastic deformation of detwinned martensite (B-C). Upon unloading, the Nb nanowires underwent a small recovery of tensile elastic deformation (B-C in Figure S7-b), the martensitic NiTi matrix underwent a small recovery of tensile elastic deformation (C-D in Figure S7-c) followed by a compressive elastic deformation of detwinned martensite (D-E in Figure S7-c).

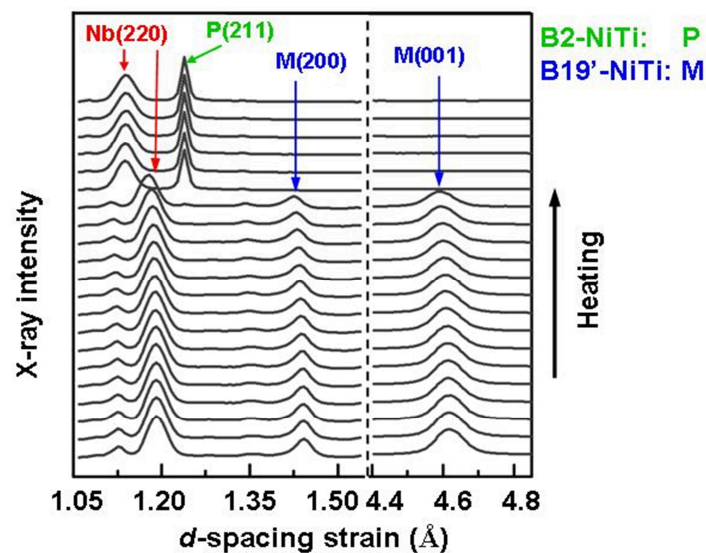


Figure S8. *In situ* synchrotron X-ray diffraction result of the composite sample pre-deformed to 8.7% in tension upon heating. Evolution of the high-energy X-ray diffraction

peaks for Nb (220), B2-NiTi (211), B19'-NiTi (200) and (001) planes during heating from 80 K to 480 K.

Note: The diffraction peaks of B19'-NiTi (001) and (220) disappear, accordingly the diffraction peak of B2-NiTi (220) appears during hearing, indicating that the martensitic NiTi matrix underwent the reverses martensitic transformation (B19'→B2).

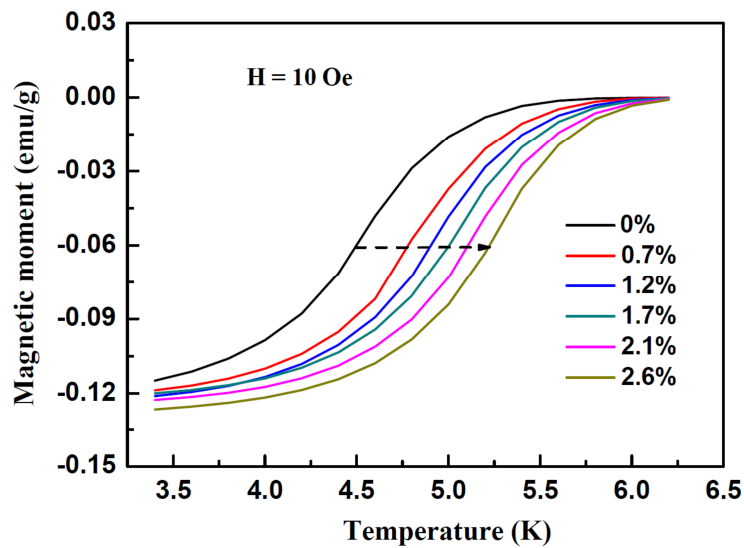


Figure S9. Superconducting transition curves of large quantity Nb nanowires subjected to different retained tensile elastic strains in freestanding composite samples. These curves are obtained on heating, after zero field cooling and then application of 10 Oe.

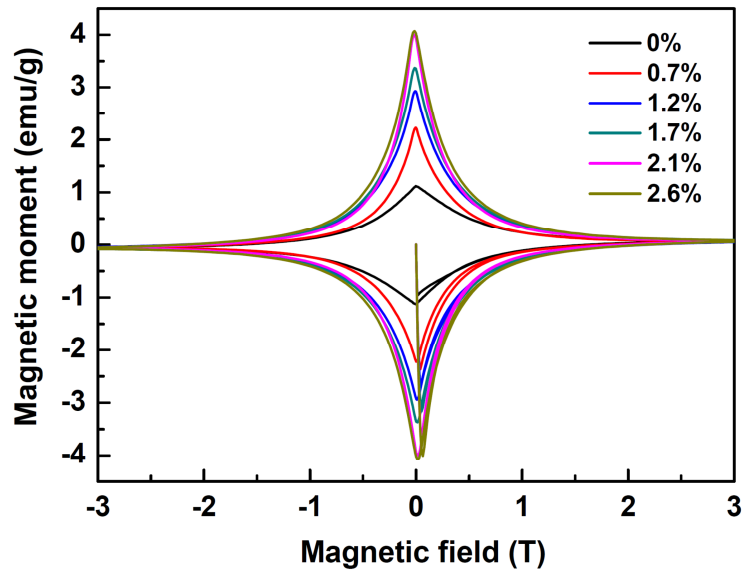


Figure S10. M-H curves of large quantity Nb nanowires subjected to different retained tensile elastic strains in freestanding composite samples measured at 2 K.